Appl. Phys. B 81, 1143–1147 (2005)
DOI: 10.1007/s00340-005-1977-0

Applied Physics B
Lasers and Optics

F. GUEYE[1]
E. SAFARI[2]
M. CHENEVIER[2]
G. GUELACHVILI[1]
N. PICQUÉ[1,✉]

Intracavity Cr^{4+}:YAG laser absorption analyzed by time-resolved Fourier transform spectroscopy

[1] Laboratoire de Photophysique Moléculaire, Unité Propre du C.N.R.S., Bâtiment 350, Université de Paris-Sud, 91405 Orsay, France
[2] Laboratoire de Spectrométrie Physique, Université J. Fourier/CNRS Grenoble, BP87, 38402 Saint Martin d'Hères Cedex, France

Received: 14 March 2005/Revised version: 5 August 2005
Published online: 4 November 2005 • © Springer-Verlag 2005

ABSTRACT A high-resolution time-resolved Fourier transform interferometer is combined with a multimode Cr^{4+}:YAG laser for intracavity laser absorption spectroscopy (ICLAS) experiments. Atmospheric absorption spectra are recorded in the 1.5 μm region with a minimum detectable absorption coefficient equal to 8×10^{-11} cm^{-1} Hz$^{-1/2}$. The broad gain bandwidth of the crystal allows a simultaneous spectral coverage at most equal to 38 nm. The laser tunability covers the 1360–1577 nm range. Water vapor detection domain extends from the 100 ppmv down to the 0.1 ppbv level.

PACS 42.62.Fi; 39.30.+w; 07.60.Ly; 33.20.Ea

1 Introduction

Intracavity laser absorption spectroscopy (ICLAS) [1] is recognized as a sensitive broadband spectroscopic technique to probe weak absorption lines from molecular or atomic gases. With ICLAS, the absorbing sample is located inside a laser cavity which has a gain bandwidth broader than the sample absorption lines. Only broadband losses are compensated by the laser gain and the laser acts for the narrow absorption lines like a multipass cell. Most often, the multimode laser is operated in long pulse mode. Then, the absorption follows the Lambert–Beer law with path length $L = ct_g$, where c is the velocity of light and t_g is the generation time, i.e. the time between the moment when population inversion reaches its threshold and the observation time. An equivalent absorption path length of several tens of kilometers can be achieved, resulting in high detection sensitivities. A major advantage of intracavity spectroscopy compared to other sensitive absorption techniques, is the simultaneous coverage of a broad spectral domain, similar to the laser gain bandwidth.

Several kinds of multimode lasers have been applied to the detection of intracavity absorption, and its application to molecular spectroscopy [2]. However, the spectral range of ICLAS application has been most often limited to the visible and very near infrared regions up to about 1 μm. In particular, Ti:Sapphire and dye lasers have been widely used to investigate the spectrum of a large variety of molecular overtone transitions. The development of ICLAS in the infrared spectral range has not been as successful yet, despite its interest for the spectroscopy of weak overtone transitions and of unstable species, and for trace gas detection. There are indeed not many broadband laser sources conveniently available in this region and multichannel grating spectrometers, which have been the traditional tool to analyze the ICLAS radiation, are also not available. Consequently, only a few demonstrations have been given, without any extensive application to spectroscopy. In particular, Co:MgF_2 at 2.047 μm [3], Tm^{3+}:YAG at 2.01 μm [4], and Cr^{2+}ZnSe at 2.5 μm [5] gain media have been implemented for intracavity spectroscopy.

The 1.3–1.6 μm near-infrared region is of particular interest. Optical fiber telecommunication industry has been the origin of important opto-electronics developments resulting in high performance and low cost devices such as semiconductor lasers or photodiodes. As the region also overlaps the J (1.1–1.4 μm) and H (1.5–1.8 μm) atmospheric windows, trace gas detectors based on laser absorption spectroscopy for application to environmental sensing [6–8] take advantage of this availability, compact sensors capable of quantitative local concentration measurements with fast response, high discrimination amongst coexisting species, and large dynamic range, are being developed. Other applications, for instance in medical diagnostics [9], and industrial process control [10], are also appearing. The important growth of applications in the near-infrared region has lead a need for fundamental spectroscopic research in order to improve both sensitive instrumental concepts and to provide molecular reference data. The latter are often missing since overtone transitions are typically four orders of magnitude weaker than fundamental bands and are often more difficult to analyze. Cavity ring-down (CRD) and photoacoustic spectroscopic schemes have been successfully implemented in this region, with minimum detectable absorption coefficient at one second averaging respectively down to 3.2×10^{-11} cm^{-1} Hz$^{-1/2}$ [9] and 3×10^{-9} cm^{-1} Hz$^{-1/2}$ [11], as well as broadband Fourier transform spectroscopy combined with multipass cells [12]. A recent example of the benefits of the application of CRD spectroscopy to parameter measurements of weak molecular lines may be found in [13].

For ICLAS development in the 1.5 μm region, the Cr^{4+} doped laser materials appear promising: they offer broad gain band and operate at room temperature. Additionally, they can

✉ Fax: 33-169-157-530, E-mail: nathalie.picque@ppm.u-psud.fr

be pumped with available solid-state, fiber, and diode lasers. In particular, the Cr^{4+}:YAG laser [14] has a tuning range between 1332 and 1554 nm [15]. It has scarcely been applied to spectroscopic purposes, most likely because its low gain makes it difficult to deal with. It has however already been demonstrated [16] with ICLA spectroscopy. A three-mirror cavity was coupled to a single-channel sequential grating spectrograph. Atmospheric water vapor spectra were obtained between 1450 and 1470 nm with generation time at most equal to 50 μs. Laser tunability and linearity of absorption path length versus generation time were not demonstrated.

For analyzing the broadband laser infrared emission spectrum, Fourier transform (FT) spectrometers appear as the most efficient instruments. High spectral resolution providing recorded lines shaped by the Doppler-limited line profile – and not by the instrument line shape – is easily attainable with commercial instruments. They only need one single detector. Furthermore, time-resolved FT interferometers [17] are available, which enable the temporal sampling of the laser transient spectral dynamics observed in the repetitive pulsed operation mode. However, FTS has not been as popular as multichannel grating spectrometers yet. There are a limited number of ICLAS measurements using FTS that have been performed, mostly in the visible region of the spectrum with dye [18, 19] and titanium-sapphire [20–22] lasers (down to 0.83 μm). To our knowledge, there are only three articles [5, 23, 24] reporting different infrared ICLAS-FTS setups. All of them benefit from time resolution, one [24] making use of a rapid scanning interferometer, and the two others [5, 23] using the same stepping-mode interferometer as the one used in this paper. Stepping-mode time resolved Fourier spectroscopy has one important advantage: the perfect separation between time and spectral dimensions, brings all time-components onto exactly the same wavenumber scale. Due to the particular nature of the stepping-mode data acquisition, these time-components share many features; the recording time, resolution, SNR, and the entire spectral range, with no need of concatenation, are identical. The results benefit from better accuracy and reduced systematic errors. Appropriate checks of the exactness of the equivalent absorbing paths through the consistency of their time evolution are then made possible.

In the present paper, the coupling of a multimode Cr^{4+}:YAG laser and a high resolution time-resolved stepping-mode Fourier transform interferometer is described. Spectra of the atmosphere of the laboratory are recorded over a broad spectral range, and the sensitivity provided by the intracavity path length enhancement is evaluated and discussed.

2 Experimental

The laser developed for intracavity spectroscopy is a strongly multimode Cr^{4+}:YAG oscillator [25]. A schematic of the experimental set-up is shown in Fig. 1. Pump light at 1064 nm from a commercial 10.5 W Nd:YVO_4 laser (Spectra-Physics) is focused by a 75 mm focal length lens into the Cr^{4+}:YAG laser crystal. Mode-matching ensures TEM_{00} operation of the Cr^{4+}:YAG laser. Modulation of the pump power is achieved with a mechanical chopper operating in the kHz frequency range. It brings the Cr^{4+}:YAG laser repetitively above and below lasing threshold. The Cr^{4+}:YAG crystal

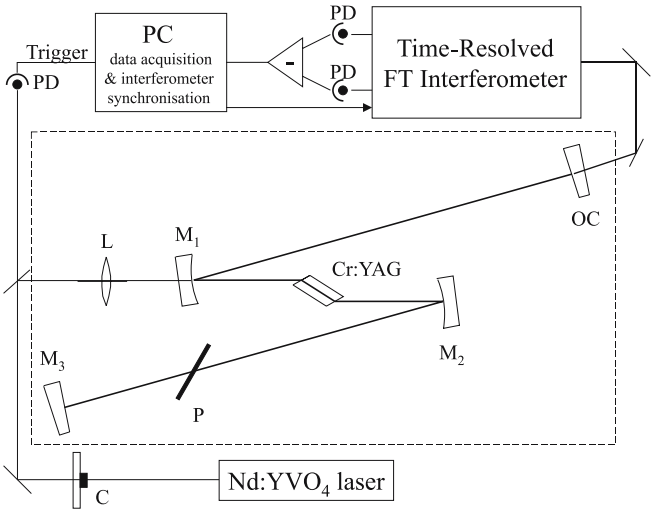

FIGURE 1 Schematic representation of the TRFT-ICLAS experimental set-up. The Cr^{4+}:YAG laser resonator is made of the highly-reflective spherical M_1, M_2, and plane M_3 mirrors and of the output coupler OC. The *dashed rectangle* represents the laser cavity enclosure that can be purged. The light leaking out the cavity is analyzed by a high resolution time-resolved Fourier interferometer and detected by two InGaAs photodetectors (PD). A personal computer (PC) holds the softsoftware and hardware for the control of the whole experimental procedure including the digitization (500 MHz/8bits) of the interferometric signal. C: chopper, L: lens, P: pellicle

is a water-cooled 2 cm-long Brewster–Brewster-cut cylindrical rod. Its small-signal absorption coefficient is 1.7 cm^{-1}. The standing-wave resonator consists of four mirrors in a Z-shaped configuration. Two 100-mm radius of curvature highly reflective concave mirrors, M_1 and M_2, on each side of the crystal provide a beam waist in the gain medium. Their reflection coefficient is 99.95% in the 1400–1600 nm range and their transmission is better than 97% at 1064 nm to let the pump beam go through M_1. The folding angle of the cavity is set at 31.5° to compensate for the astigmatism of the rod. The laser cavity is completed with a flat high reflector, M_3, and a flat output coupler, OC, with 0.5% transmission. Both arms (M_1-OC, M_2-M_3) are about 25 cm long. The laser may be tuned by slightly rotating a 2-μm-thick uncoated nitrocellulose pellicle P around the Brewster-angled orientation. The CW lasing threshold is at the lowest 0.8 W of pumping power. The Cr^{4+}:YAG resonator is enclosed in an air-tight chamber, with two windows for the optical connections (pump and output beams). The output beam is optically conjugated to a time-resolved Fourier transform spectrometer.

The spectrometer is a home-made Connes-type Michelson interferometer. Details of its performances for high resolution spectroscopy and time-resolved studies may be found in [17, 26, 27]. Summarizing, the interferometer is a stepping-mode interferometer. In Fourier spectroscopy, the wavenumbers ν in the spectrum and the path difference Δ in the interferogram are related by the Fourier transform. Consequently, in order to get an accurate wavenumber scale and to avoid systematical effects which distort the spectra, Δ must be accurately determined. A 3.39 μm methane-lamb-dip stabilized HeNe laser is used as a reference for the servo-control scheme. The control of the position of the cat's eye assembly of the moving arm of our interferometer is used to phase-lock Δ within peak-to-peak

maximum fluctuations smaller than 1 nm at any absolute value between 0 and 2 meters. The interferometer operates under a primary vacuum, which both improves path difference determination by removing errors induced by the air index, and eliminates atmospheric absorption and turbulences. Wavenumber relative accuracy and precision respectively better than 5×10^{-9} [12] and 4×10^{-10} [28] have been demonstrated using this instrument. Time and spectral resolutions are user selectable with uppermost values respectively equal to 2 ns and $2.5 \times 10^{-3}\,\mathrm{cm}^{-1}$. Stepping-mode operation ensures complete decorrelation between time sampling and mirror motion for path difference excursion. It eliminates systematical effects and allows better time resolution and observation duration capabilities combined with simpler synchronization schemes than with rapid-scan interferometers.

In the present experiments, the time-resolved Fourier transform spectrometer is equipped with an infrasil beamsplitter and two InGaAs photodetectors at its output ports. As in all ICLAS-TRFTS experiments performed at LPPM [5, 23], the laser is operated in a long-pulse ($\sim 500\,\mu$s) repetitive and periodic mode. At a given path difference step, a photodiode monitoring the pump beam radiation triggers the temporal sampling of the Cr^{4+}:YAG laser pulse interferometric signal. Several laser pulses may be co-added to increase the signal-to-noise ratio (SNR). Then the cat's eye assembly of the moving arm of the interferometer proceeds to the next step, and so on up to the desired maximum path difference. Note retro-reflectors are especially useful when analyzing laser sources since proper optical alignment allows avoidance of any feedback in the laser resonator. At the end of an experiment, as many time-component interferograms as time-samples of one laser pulse are obtained. Each of them produces a spectrum with a well defined laser generation time. In the present experiments, from 64 up to 256 time samples are acquired. At a given path difference step, several (from 1 to 256) laser pulses are also co-added. Time resolution is chosen between 3.2 μs and 0.32 μs.

3 Results and discussion

In order to characterize the experimental setup, spectra of the laboratory atmosphere have been recorded with the laser enclosure either purged or not with dry nitrogen. Figure 2 presents four time-components from a 128-components spectrum, made without any tuning element inserted in the resonator. The laser emission is centered at 1.451 μm. The pump parameter η, i.e. the ratio of the pump power to its threshold value, is equal to 1.3 and the chopper frequency is set to 1 kHz. The present spectrum is recorded after six hours of dry nitrogen purge. It is however still over-saturated with water absorption lines. The explored spectral domain is indeed the location of the $2\nu_1$ and $2\nu_2 + \nu_3$ strong vibration–rotation H_2O bands [29]. At each given path difference step, 128 time samples are taken from a given laser pulse with a 3.2 μs time-resolution and 32 pulses are averaged to improve the SNR. The data acquisition procedure results in a 128 time-components spectrum. Each time-component made of 10 000 spectral elements covers 339 nm ($1475\,\mathrm{cm}^{-1}$). Unapodized instrumental spectral resolution is equal to 31 pm ($0.15\,\mathrm{cm}^{-1}$), similar to the width of the air-broadened water lines. The laser spectral emission domain covered by the small t_g time components is at most 38 nm ($175\,\mathrm{cm}^{-1}$) for generation times of about 25 μs. Although this does not appear clearly in Fig. 2 due to the laser intensity dynamic evolution, the spectral narrowing reduces this spectral range by a factor of about 2.5 for the longest sampled t_g equal to about 440 μs (129 km equivalent absorbing path).

The laser can be tuned by inserting a nitrocellulose pellicle into the resonator in a Brewster-angled orientation. The

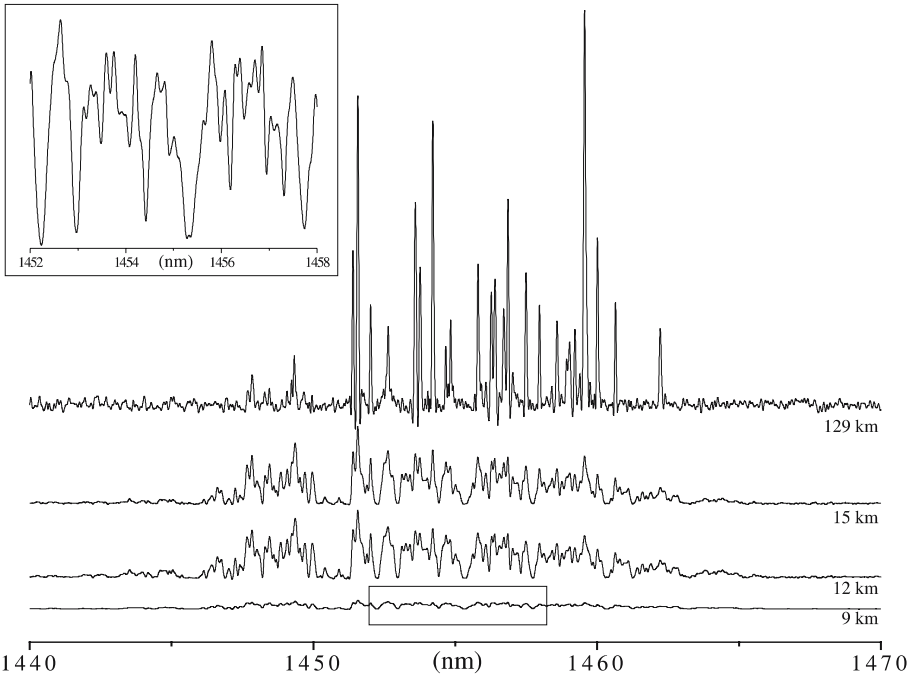

FIGURE 2 Four components (generation times: 30, 40, 50, 430 μs) of a water vapor absorption time-resolved spectrum in the 1455 nm region obtained after N_2-purging of the laser enclosure for six hours. The upper *inset* provides an expanded view of the surrounded portion of the 30 μs-generation time time-component spectrum. Total recording time is 7 minutes. Peak looking features in the longest absorption path component indicate possible atmospheric microwindows

laser emission bandwidth is then reduced by a factor of about 3 down to 14 nm (60 cm^{-1}) at broadest, for low generation times. In practice, tunability between 1360 and 1577 nm (6340–7350 cm^{-1}) is obtained. Figure 3 provides an example of an atmospheric absorption time-resolved spectrum when tuning the laser at 1535 nm. The 128 time-components which are sampled are displayed. As atmospheric water vapor absorption is weaker in this region, the laser enclosure was not purged. The absorption rotational lines belong to the $\nu_1 + 2\nu_2$ and $2\nu_2 + \nu_3$ bands [29], with individual intensities in the 10^{-24}–10^{-25} cm molecule^{-1} range. The pump parameter η is 1.5 and the chopper frequency 1.2 kHz. Time resolution is 3.2 μs. Sixteen co-additions are performed. Each time-component is made of 20 000 spectral elements and covers 169.5 nm (737.5 cm^{-1}). Unapodized spectral resolution is equal to 8.7 pm (0.037 cm^{-1}), whereas the air-broadened width of the water lines is of the order of 20 pm. Absorption path length extends from 3.6 up to 126.5 km.The insert in Fig. 3 gives a representation of time sample number seven, exhibiting 9.3 km absorption path length. In order to check that the law $L = ct_g$ is indeed valid for the present measurements, the evolution of the absorbance versus generation time has been plotted in Fig. 4 for two lines, respectively centered at 1533.27 and 1533.84 nm. Absorbance is approximated as being $\alpha L \approx -\ln(1 - I_a/I_0)$, where α is the absorption coefficient, I_a is the peak absorption at line center, and I_0 is the local background. The two lines were not overlapped by neighbors. Their intensities of the order of 10^{-25} cm molecule^{-1} enabled intense enough observation of them at low generation times and unsaturated at high generation times. The good linearity of absorbance, in these over-saturated spectra, validates the linear correspondence between generation time and absorption path length.

The sensitivity which is reached with the present experimental setup may be estimated in the following way. Taking for instance the recording conditions of the time-resolved spectrum shown on Fig. 2, the highest equivalent absorbing

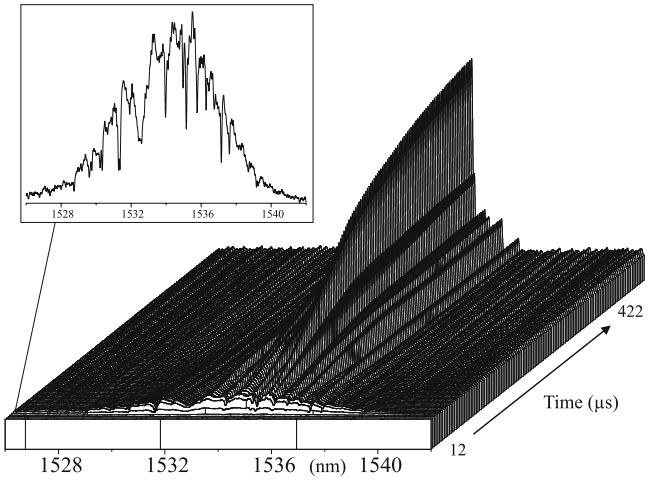

FIGURE 3 Atmospheric absorption time-resolved spectrum made of 128 time-components. The laser is tuned in the 1535 nm region. Two consecutive components are 3.2 μs from each other. This corresponds to a 960-meter increase of the equivalent absorbing path L. Spectral resolution is 8.7 pm (0.037 cm−1). Total recording time is 9 minutes. The enclosure displays time-component number 7

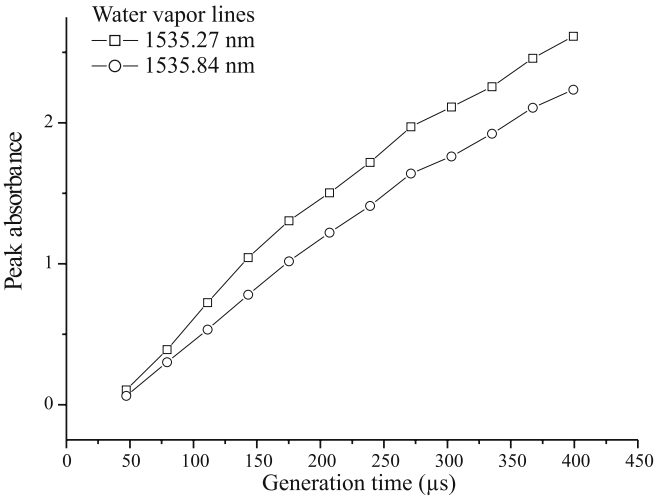

FIGURE 4 Variation of the peak absorbance of two water absorption lines centered at 1533.27 and 1533.84 nm versus generation time. Even with an absorbance determination degraded by the increased perturbation of the neighboring lines at high generation times, the linear evolution of the absorption path with the generation time, does not show any dramatic tendency to saturation

path L reached in the present experiments is equal to 129 km. With a SNR ratio of about 50, the corresponding minimum detectable absorption coefficient α_{min}, equal to $1/(\mathrm{SNR} \times L)$, is 1.5×10^{-9} cm^{-1}. Thanks to Fourier transform spectroscopy, a total of about 1.3×10^6 spectral elements are measured, among which only 150 000 report the laser emission restricted range. Consequently, with a total recording time equal to seven minutes, the minimum detectable absorption coefficient at 1-second time averaging is 8×10^{-11} $cm^{-1}Hz^{-1/2}$ per spectral element. The most intense H_2O observed line, not shown on the figure, is located at 1368.6 nm (7306.7521 cm^{-1}). Its intensity is 0.450 $cm^{-2}atm^{-1}$ (1.795×10^{-20} cm molecule^{-1}) at 296 K [30]. Knowing that with a Doppler lineshape, the percent transmission at the center of the line is given [31] by $100\exp(-CSlp/\gamma_D)$, where C is a numerical factor equal to 1.1494×10^{14}, S is the line intensity in units of cm molecule^{-1}, l is the path length in cm (1.3×10^7), p the pressure in Pa and γ_D the line half-width in cm^{-1} (0.01), the H_2O detection limit is reached when using this line, for a pressure equal to 40 Pa. In a low pressure environment, the 1.5×10^{-9} cm^{-1} minimum detectable absorption coefficient then corresponds to 0.10 ppbv water vapor detection limit. In an atmospheric pressure environment, using a similar formula [31] with pressure-broadened lineshape ($C = 7.789 \times 10^{13}$, $\gamma = 0.075$ cm^{-1}), the water vapor detection limit is 1 ppbv. Such stringent detection limits fit the particular need for moisture detection in the semiconductor fabrication industry. Note that the present experiment could also be useful to accurately determine microwindows, free of atmospheric water vapor absorption, as it is needed for instance, for free space optics and telecommunications. Additionally, thanks to the tunability of our device, the demonstrated detection range extends up to the 100 ppmv domain. In the perspective of trace gas detection, the diode pumping possibility [32] would considerably reduce the price of the equipment together with increasing its compact size. However, as far as laboratory spectroscopy is

concerned, even a long dry nitrogen purge appears to be insufficient to remove satisfactorily atmospheric water vapor lines. Installing the laser under vacuum is already undertaken. As performed recently with a Cr^{2+}:ZnSe laser [5], getting the operation of the laser in a low-pressure gas filled enclosure after secondary-vacuum evacuation, should actually be the most effective solution to achieve higher quality laboratory spectra.

REFERENCES

1 V.M. Baev, T. Latz, P.E. Toschek, Appl. Phys. B **69**, 171 (1999)
2 M. Herman, J. Lievin, J. Vander Auwera, A. Campargue, *Global and Accurate Vibration Hamiltonians from High-Resolution Molecular Spectroscopy*, Advances in Chemical Physics, I. Prigogine, S.A. Rice (Eds.) (Wiley, 108, 1999)
3 M.P. Frolov, Y.P. Podmar'kov, Opt. Comm. **155**, 313 (1998)
4 J. Geng, J.I. Lunine, G.H. Atkinson, Appl. Opt. **40**, 2551 (2001)
5 N. Picqué, F. Gueye, G. Guelachvili, E. Sorokin, I. Sorokina, Opt. Lett. **30**(24), (15 december 2005)
6 S. Barrass, Y. Gérard, R.J. Holdsworth, P.A. Martin, Spectrochimica Acta Part A: Molecular and Biomolecular Spectroscopy **60**, 3353 (2004)
7 E.C. Richard, K.K. Kelly, R.H. Winkler, R. Wilson, T.L. Thompson, R.J. McLaughlin, A.L. Schmeltekopf, A.F. Tuck, Appl. Phys. B **75**, 183 (2002)
8 G. Durry, A. Hauchecorne, J. Ovarlez, H. Ovarlez, I. Pouchet, V. Zeninari, B. Parvitte, J. Atmosph. Chem. **43**, 175 (2002)
9 E.R. Crosson, K.N. Ricci, B.A. Richman, F.C. Chilese, T.G. Owano, R.A. Provencal, M.W. Todd, J. Glasser, A.A. Kachanov, B.A. Paldus, T.G. Spence, R.N. Zare, Analyt. Chem. **74**, 2003 (2002)
10 J.B. Dudek, P.B. Tarsa, A. Velasquez, M. Wladyslawski, P. Rabinowitz, K.K. Lehmann, Analyt. Chem. **75**, 4599 (2003)
11 M.E. Webber, M. Pushkarsky, C. Kumar, N. Patel, Appl. Opt. **42**, 2119 (2003)
12 N. Picqué, G. Guelachvili, J. Mol. Spectros. **185**, 244 (1997)
13 P. Macko, D. Romanini, S.N. Mikhailenko, O.V. Naumenko, S. Kassi, A. Jenouvrier, V.G. Tyuterev, A. Campargue, J. Mol. Spectros. **227**, 90 (2004)
14 N.B. Angert, N.I. Borodin, V.M. Garmash, V.A. Zhitnyuk, A.G. Okhrimchuk, O.G. Siyuchenko, A.V. Shestakov, Sov. J. Quantum Electron. **18**, 73 (1988)
15 D. Welford, M.A. Jaspan, J. Opt. Soc. Am. B **21**, 2137 (2004)
16 D.A. Gilmore, C. Vujkovic, G.H. Atkinson, Opt. Comm. **103**, 370 (1993)
17 N. Picqué, G. Guelachvili, Appl. Opt. **39**, 3984 (2000)
18 C. Domingo, A. del Olmo, R. Escribano, D. Bermejo, J.M. Orza, J. Chem. Phys. **96**, 972 (1992)
19 K. Strong, T.J. Johnson, G.W. Harris, Appl. Opt. **36**, 8533 (1997)
20 C. Depiesse, G. Di Lonardo, A. Fayt, L. Fusina, D. Hurtmans, S. Robert, F. Tamassia, J. Vander Auwera, A. Baldan, M. Herman, J. Mol. Spectros. **229**, 137 (2005)
21 S.M. Hu, A. Campargue, Z.Y. Wu, Y. Ding, A.W. Liu, Q.S. Zhu, Chem. Phys. Lett. **372**, 659 (2003)
22 S. Yang, M. Metsälä, T. Lantta, P. Suero, R. Martinez, O. Vaittinen, L. Halonen, Chem. Phys. Lett. **396**, 213 (2004)
23 N. Picqué, G. Guelachvili, A.A. Kachanov, Opt. Lett. **28**, 313 (2003)
24 A. Stark, L. Correia, M. Teichmann, S. Salewski, C. Larsen, V.M. Baev, P.E. Toschek, Opt. Commun. **215**, 113 (2003)
25 E. Safari, Thèse de Doctorat en sciences, Université Joseph Fourier (Grenoble), 2002
26 J. Connes, H. Delouis, P. Connes, G. Guelachvili, J.P. Maillard, G. Michel., Nouv. Rev. Opt. Appl. **1**, 3 (1970)
27 G. Guelachvili, Appl. Opt. **17**, 1322 (1978)
28 G. Guelachvili, Appl. Opt. **20**, 2121 (1981)
29 L.S. Rothman, A. Barbe, D.C. Benner, L.R. Brown, C. Camy-Peyret, M.R. Carleer, K. Chance, C. Clerbaux, V. Dana, V.M. Devi, A. Fayt, J.M. Flaud, R.R. Gamache, A. Goldman, D. Jacquemart, K.W. Jucks, W.J. Lafferty, J.Y. Mandin, S.T. Massie, V. Nemtchinov, D.A. Newnham, A. Perrin, C.P. Rinsland, J. Schroeder, K.M. Smith, M.A.H. Smith, K. Tang, R.A. Toth, J. Vander Auwera, P. Varanasi, K. Yoshino, J. Quant. Spectros. Radiat. Transfer **82**, 5 (2003)
30 R.A. Toth, Appl. Opt. **33**, 4851 (1994)
31 A.G. Maki, J.S. Wells, NIST, Washington, DC, USA, Spec. Publ. **821**, pp. 1–645 (1991)
32 S. Naumov, E. Sorokin, I.T. Sorokina, Opt. Lett. **29**, 1276 (2004)